Polymer Degradation and Stability 97 (2012) 1485–1494

Contents lists available at SciVerse ScienceDirect

Polymer Degradation and Stability

journal homepage: www.elsevier.com/locate/polydegstab

The effect of oxygen on the irradiation process of ethylene–butene copolymer

Marcelo D. Failla [1], Adriana Brandolin [1], Claudia Sarmoria*, Enrique M. Vallés [1]

Planta Piloto de Ingeniería Química (PLAPIQUI – UNS – CONICET) CC 717, 8000 Bahía Blanca, Argentina

ARTICLE INFO

Article history:
Received 5 December 2011
Received in revised form
4 April 2012
Accepted 11 May 2012
Available online 26 May 2012

Keywords:
Polyethylene
Gamma irradiation
Oxygen
Mathematical model

ABSTRACT

A model ethylene–butene copolymer of narrow molecular weight distribution was irradiated with γ-rays under different oxygen-containing atmospheres. Gel fraction, carbonyl content and molecular weights were measured. Weight average molecular weights have been measured for all pregel samples and for the sol fraction of the postgel samples. Two different regimes seem to be present. Early on, molecular weight decreases with irradiation dose. At a later stage, further irradiation leads to a molecular weight increase. The dose at which this change of regime takes place varies with the oxygen concentration in the processing atmosphere. We have modeled this process assuming that oxygen is consumed at the early stages of irradiation, and that the variable that triggers the difference in response is the presence or absence of oxygen. Good agreement with measured values is found using either a probability model or a kinetic model.

1. Introduction

It has been observed in the past that irradiation of polyethylenes in the presence of oxygen leads to results different from those found when irradiating under vacuum. When oxygen is present it is consumed, oxidation products may be measured both in the polymer and in gaseous effluents, and the polymer molecular weight tends to decrease [1–5]. Under vacuum, no oxidation products are measurable and irradiation leads to increasing molecular weights [3,6,7].

The oxidation products in polyethylenes irradiated in the presence of oxygen have been found to contain mainly carbonyl, hydroxyl and peroxide groups. In the detailed study that Decker et al. [8] performed on the irradiation of polyethylene and other polyolefins in the presence of excess oxygen, the main oxidation products found were hydroperoxides, dialkyl peroxides and carbonyl-containing molecules. These three types of molecules accounted for over 85% of the consumed oxygen. The remaining oxidation products were assumed to be alcohols and volatiles. These experimental results were revisited by Khelidj et al. [9], who proposed a kinetic mechanism that could be used to describe the observed results. More recently, Buttafava et al. [10] irradiated thin films of commercial LLDPE in air at room temperature using three different dose rates. They detected the formation of hydroperoxides and carbonyls, in quantities that decreased with dose rate. In view of their experimental findings, they propose that peroxyradicals and alkyl radicals coexist in a quasi-stationary state under the control of the competition between propagation and termination reactions.

Irradiation-induced oxidation has been reported to depend on the crystallinity of the polymer [4,5,11–13], oxygen diffusion [1,2,4], the presence of antioxidant or antirad agents [3,14], and total dose. Several authors have concluded that irradiation rate is also an important variable, although at least in some cases this could be assimilated to the effect of oxygen diffusion, since lower irradiation rates allow time for oxygen to diffuse into the samples [15].

Babić [16,17] reported results on irradiation of commercial polyethylenes in the presence of air absorbed in the samples, where he found that molecular weights decreased at low doses to later increase again as irradiation proceeded further. He applied a correction to the Charlesby–Pinner theory to be able to fit gel fraction as a function of irradiation dose [17], where he had to consider different crosslinking and scission rates at different stages in the irradiation process. He did not report modeling average molecular weights, nor information on the effect of other oxygen contents in the atmosphere.

The fact that commercial polyolefins have a relatively wide molecular weight distribution makes analysis of the results of irradiation rather complex. Some of us [7,18,19] have shown in the past that the use of model polyolefins of narrow molecular weight distribution is a very helpful aid when elucidating the mechanisms

* Corresponding author. Tel.: +54 291 4861700; fax: +54 291 4861600.
E-mail addresses: mfailla@plapiqui.edu.ar (M.D. Failla), csarmoria@plapiqui.edu.ar (C. Sarmoria).
[1] Tel.: +54 291 4861700; fax: +54 291 4861600.

0141-3910/$ – see front matter © 2012 Elsevier Ltd. All rights reserved.
doi:10.1016/j.polymdegradstab.2012.05.004

present in irradiation, as any uncertainty related to the initial molecular weight distribution is eliminated. The aim of this work is to determine the influence of the oxygen content of the environment on an irradiated model resin. We present results on irradiation of ethylene–butene copolymers of narrow molecular weight distributions under different atmospheres, initially containing anywhere from 0% to 100% oxygen, all at the same irradiation rate. We attempt to explain the influence of oxygen content and its consumption on the resulting molecular weights, and propose two mathematical models to explain the observed behavior.

2. Experimental

2.1. Polymer synthesis

A linear polybutadiene (PB) was synthesized by anionic polymerization of butadiene under high purity conditions following standard methods [20–22]. The polymerization was carried out in cyclohexane solution, under high vacuum and at room temperature. The reaction was initiated with tertiary butyl–lithium, and isopropanol was the termination reagent. Infrared spectroscopy (IR) was used to determine the double bond microstructure of the PB's. The IR spectra of the samples, which were obtained using a Nicolet 520FT-IR spectrometer, revealed that about 7% of the butadiene molecules were incorporated to the growing chain following a 1,2-addition path.

The synthesized polybutadiene was subsequently hydrogenated in toluene solution using a Pd supported catalyst. The hydrogenation was performed in a Parr reactor at 90 °C and 700 psi. The hydrogenation method and conditions were similar to the ones used by Rachapudy et al. [21]. In order to estimate residual unsaturations after the hydrogenation step, IR spectra of the hydrogenated polybutadiene (HPB) were recorded at room temperature on 0.1 mm-thick films. The absorption peaks at 910 cm^{-1} and 966 cm^{-1} were monitored, as they are associated to vinyl and trans groups, respectively. We found no evidence of absorption bands that could be associated to double bonds. This confirmed that a highly saturated hydrocarbon polymer was obtained after hydrogenation. The resulting HPB has a molecular structure chemically similar to a random ethylene-(1-butene) copolymer with a composition of about 20 CH_3/1000 C. This can be inferred from the level of 1,2-addition of butadiene (~7% mol/mol) measured in the original PB.

2.2. Sample preparation

Films of the starting material with thickness of 0.1 ± 0.01 mm were prepared by compression molding at 150 °C using a hydraulic press with thermostatically controlled platens. The samples were molded between 1.5 mm thick steel plates held apart by 0.1 mm thick brass spacers.

2.3. Irradiation procedure

The films were inserted into glass Pyrex tubes of 15 ml. All tubes contained approximately the same total mass. The tubes were evacuated to 10^{-4} torr for 2 days, then filled with different mixtures of oxygen/nitrogen and sealed off. The mixtures used had oxygen concentrations of 0, 25, 50, 75 and 100% v/v and a total pressure of 1 atm at room temperature. Subsequently these sealed tubes were exposed to γ-rays generated by a ^{60}Co source. The treatment was performed at room temperature, using a dose rate of 8 kGy/h as determined by a radiochromic thin-film dosimeter. Doses ranging from 20 to 200 kGy were applied to the samples. The error in dose measurement is estimated to be 5%.

2.4. Sample analysis

The gel fraction was determined by extraction of solubles with xylene at 125 °C. The extraction was performed by placing about 30 mg of sample into a stainless steel mesh basket, and immersing it in hot xylene for periods of 6 h. An antioxidant, Irganox 1010, was added to the xylene solution to prevent the propagation of oxidation reactions initiated by radicals produced by the decomposition of peroxide groups that may have formed during irradiation. After each 6 h period the samples were dried to constant weight in a vacuum oven at 60 °C. The process was repeated until no weight change was detectable in the dry gel after two consecutive extraction periods. The total time of extraction varied between 36 h and 48 h depending on the sample. Fresh solvent was used in each extraction period. The soluble fraction that remained in the xylene solution was subjected to molecular weight measurement.

Size Exclusion Chromatography (SEC) was used to determine the molecular weights and molecular weight distributions of all soluble samples – the entire sample in the pregel region, and the sol fraction only in the postgel region. The instrument used was a Waters 150-C ALP/GPC with two detectors: an internal refractive index (RI) detector and an on-line Multi Angle Light Scattering detector (LS) from Wyatt Technology (Dawn DSP). The SEC measurements were performed at 135 °C using 1,2,4 trichlorobenzene as solvent and a set of five PLGel columns from Polymer Labs with nominal pore sizes of $10^6, 10^5, 10^4, 10^3$ and 500 Å. The average molecular weights, Mn and Mw, were estimated using the ASTRA program provided by Wyatt Technology Corp. The measured average molecular weights are reported in Table 1.

All materials were studied by means of Fourier Transform Infrared (FTIR) spectroscopy. The FTIR spectrum was recorded in transmission mode with a 4 cm^{-1} resolution using a Nicolet 520 spectrometer. The region of the spectrum analyzed was between 1800 and 1650 cm^{-1}, where absorption bands associated to carbonyl groups appear as a result of oxidative degradation [23]. With the aim of comparing the samples in terms of their oxidation degrees, a carbonyl index was defined as the total area of the absorption bands (1800–1650 cm^{-1}) divided by the film thickness. This is the same index used by other authors to follow the built-up of carbonyl groups in polyethylene [10,24,25].

Table 1
Average molecular weights from GPC-MALLS. Postgel measurements are reported in boldface.

Sample	Dose (kGy)	M_n (g/mol)	M_w (g/mol)
Nitrogen	0	65,500	72,000
	29	108,800	199,000
	56	**101,500**	**179,500**
	138	**47,000**	**67,300**
21% Oxygen	29	32,600	53,300
	56	59,300	138,300
	84	61,700	151,700
	138	**59,000**	**159,500**
50% Oxygen	34	43,600	60,700
	69	27,000	44,000
	136	32,200	72,400
	170	**20,000**	**42,000**
75% Oxygen	34	38,600	55,700
	69	27,500	44,000
	103	21,500	35,000
	136	17,600	38,300
	203	**20,900**	**44,500**
100% Oxygen	34	43,300	59,900
	69	31,200	49,000
	103	19,600	30,000
	136	24,000	83,600
	203	**18,700**	**41,700**

3. Mathematical modeling

This system was modeled using two different approaches: a probability model and a kinetic model. The probability model allows calculations both in the pregel and postgel regions, given the relative rates of crosslinking and scission. The kinetic model, although restricted to the pregel region, allows more insight in the reaction mechanism.

3.1. Probability model

We used an extension of a previous model that considered simultaneous crosslinking and scission reactions of polymer chains [18,26]. In the previous model it was assumed that all C–C bonds were equally likely to be subject to crosslinking or scission, that all reactions were independent, and that no intramolecular reactions were possible. In that model two conversions were defined: α, for crosslinking reactions, and β, for scission reactions, where $0 \leq \alpha \leq 1$, $0 \leq \beta \leq 1$. Because reactions are independent, considering crosslinking and scission as simultaneous events or sequential steps gives the same final result. The model considers sequential steps: only scission up to conversion β first, followed by crosslinking of the resulting polydisperse chains up to conversion α. All of these characteristics were kept for the current model. The change introduced in this work concerns the specification of conversions α and β. In the previous model the specification was one for the entire range of applied doses: either crosslinking or scission predominated at all doses. This no longer applies in this work, because the atmosphere changes as the treatment advances and oxygen is consumed in the sealed glass ampoules. It has been documented that scission predominates when irradiating polyethylene in the presence of oxygen, but crosslinking is more important in oxygen-free environments. For the samples irradiated under vacuum, we only observed molecular weights that increased with dose until a gel was formed. For the remaining samples, the experimentally measured weight average molecular weights in this work showed a period of decrease with dose, consistent with a predominance of scission, followed by an increase with dose leading to a gel, consistent with a predominance of crosslinking. In view of this behavior the model must consider at least two different regimes. In order to tackle this situation, we introduced the possibility of specifying several exposure periods where different rules would apply for the two conversions. This requires the introduction of an extra parameter, the irradiation dose at which the regime changes. In both zones a linear function of α with dose was chosen. The same parameters were used for all samples; only the boundary between regime regions was changed for each initial atmospheric composition.

$$\beta = \begin{cases} P_{b1} D & \text{if } D < D_{\mathrm{ch},i} \\ P_{b1} D_{\mathrm{ch},i} & \text{if } D \geq D_{\mathrm{ch},i} \end{cases} \quad (1)$$

$$\alpha = \begin{cases} P_{a1} D & \text{if } D < D_{\mathrm{ch},i} \\ P_{a1} D_{\mathrm{ch},i} + P_{a2} (D - D_{\mathrm{ch},i}) & \text{if } D \geq D_{\mathrm{ch},i} \end{cases} \quad (2)$$

In these expressions D is the dose in kGy, $D_{\mathrm{ch,i}}$ is the dose at which the regime changes for the ith initial atmospheric composition, while P_{a1}, P_{a2}, and P_{b1} are proportionality constants to be fitted to experimental data. Equation (1) indicates that the degree of scission β remains constant for $D \geq D_{\mathrm{ch,i}}$, implying that in oxygen-free atmospheres there is no scission. This is a simplifying approximation. Previous work in our group [18,27] has shown that monodisperse HPB irradiated under vacuum undergoes low levels of scission, with a maximum of 5 scission events per 100 crosslinking events. Since such low scission levels may be safely ignored when modeling average molecular properties, we have allowed scission only in oxygen-containing atmospheres.

3.2. Kinetic model

We assumed that the polymer film is surrounded by a gas composed by oxygen and nitrogen. Volumes of the solid and gas phases are considered to be equal. At the beginning of the irradiation process, the film is considered to be saturated with oxygen. As long as the gas phase contains enough oxygen, we consider this phase as a reservoir capable of providing oxygen to the film phase at a rate that exactly equals that of consumption. Once saturation in the film phase can no longer be maintained, oxygen diffusion is considered explicitly in the model.

3.2.1. Reaction mechanism

A mechanism for the γ-irradiation of PE at room temperature in the presence of oxygen is proposed, based on a previous kinetic mechanism proposed for peroxide modification of PE [28] and modified to account for γ-radiation. New reactions were added to the mechanism to account for the effect of oxygen on the modification process. The reaction selection was based on published experimental findings [8,10], our own measurements, and mechanistic considerations [9]. In the mentioned works, carbonyls and hydroperoxides were measured in experiments where irradiation was performed on PE samples under air. In consequence, the mentioned species should be part of any proposed mechanism. On the other hand, it would appear that for a proper description of the experiments it is necessary to consider that not all of the combination reactions result in dead polymer [9]. More details regarding the experimental measurements that support our proposed kinetic mechanism are presented in the next section.

Taking into account the above discussion, we made the following considerations about the kinetic mechanism applicable to our particular experimental conditions:

a) Starting polymer molecules (P_n) may have any length ($n = 1 \ldots \infty$)
b) During the γ-irradiation process some polymer chains acquire oxygen groups. However, for modeling purposes simple homopolymer chains and those containing a given number (k) of hydroperoxide groups (macrohydroperoxides, $P_n(\mathrm{OOH})_k$), carbonyl groups ($P_n(=O)_k$) or hydroxyl groups ($P_n(\mathrm{OH})_k$) will all be denoted as P_n.
c) When the γ-irradiation process starts, it causes hydrogen abstraction from polymer molecules producing backbone radicals (Equation (3)), which maintain the number (n) of monomeric units (R_n, $n = 1 \ldots \infty$).
d) Macroradicals contain only one active site, since their high reactivity leads them to react rapidly.
e) While oxygen is present, the backbone radicals react preferentially with the oxygen molecules present in the polymer film to form peroxy-macroradicals (R_nO_2, $n = 1 \ldots \infty$) (Equation (4)).
f) Afterward, recombination of peroxy-macroradicals produces oxy-macroradicals ($R_n\mathrm{O}$, $n = 1 \ldots \infty$) (Equation (5)).
g) Oxy-macroradicals may suffer scission reactions leading to dead polymer and macroradical molecules (Equation (6)).
h) Macroradicals and peroxy-macroradicals may undergo termination by combination among themselves (Equations (7) and (8)) or with each other (Equation (9)). They also participate in the corresponding disproportionation reactions (Equations (10)–(12)).
i) All three types of macroradicals may suffer transfer to polymer reactions (Equations (13)–(15)).

The proposed kinetic mechanism is shown below (Equations (3)–(15)).

Hydrogen Abstraction by γ-radiation

$$P_n + \gamma_{rad} \xrightarrow{nk_{\gamma a}} R_n; n = 1, \ldots \infty \quad (3)$$

Formation of Peroxy-macroradicals

$$R_n + O_2 \xrightarrow{k_{or}} R_nO_2; n = 1, \ldots \infty \quad (4)$$

Recombination of Peroxy-macroradicals

$$R_nO_2 + R_mO_2 \xrightarrow{k_{roo}} R_nO + R_mO + O_2; n = 1, \ldots \infty;\ m = 1, \ldots \infty \quad (5)$$

Scission

$$R_nO \xrightarrow{k_{eo}} R_{n-m} + P_m; n = 2, \ldots \infty \quad (6)$$

Termination by Combination between Backbone Macroradicals

$$R_n + R_m \xrightarrow{k_{trr}} P_{n+m}; n = 1, \ldots \infty;\ m = 1, \ldots \infty \quad (7)$$

Termination by Combination between Peroxide Macroradicals

$$R_nO_2 + R_mO_2 \xrightarrow{k_{too}} P_{n+m} + O_2; n = 1, \ldots \infty;\ m = 1, \ldots \infty \quad (8)$$

Cross-termination by Combination between Peroxy-macroradicals and Backbone-macroradicals

$$R_nO_2 + R_m \xrightarrow{k_{tor}} P_{n+m} n = 1, \ldots \infty;\ m = 1, \ldots \infty \quad (9)$$

Termination by Disproportionation between Backbone Macroradicals

$$R_n + R_m \xrightarrow{k_{drr}} P_n + P_m; n = 1, \ldots \infty;\ m = 1, \ldots \infty \quad (10)$$

Termination by Disproportionation between Peroxide Macroradicals

$$R_nO_2 + R_mO_2 \xrightarrow{k_{doo}} P_n + P_m + O_2; n = 1, \ldots \infty;\ m = 1, \ldots \infty \quad (11)$$

Cross-termination by Disproportionation between Peroxy-macroradical and Backbone-macroradicals

$$R_nO_2 + R_m \xrightarrow{k_{dor}} P_n + P_m; n = 1, \ldots \infty;\ m = 1, \ldots \infty \quad (12)$$

Backbone-macroradical Chain Transfer to Polymer

$$P_n + R_m \xrightarrow{nk_{tpr}} R_n + P_m; n = 1, \ldots \infty;\ m = 1, \ldots \infty \quad (13)$$

Peroxy-macroradical Chain Transfer to Polymer

$$P_n + R_mO_2 \xrightarrow{nk_{tpo}} R_n + P_m; n = 1, \ldots \infty;\ m = 1, \ldots \infty \quad (14)$$

Oxy-macroradical Chain Transfer to Polymer

$$P_n + R_mO \xrightarrow{nk_{tps}} R_n + P_m; n = 1, \ldots \infty;\ m = 1, \ldots \infty \quad (15)$$

In the above equations P stands for polymer molecules, R for backbone macroradicals, RO_2 for peroxy-macroradicals and RO for oxy-macroradicals. The subscript or index that accompanies them indicates their degree of polymerization. Each kinetic constant (k) is identified with a subscript. Constants given in molar units appear alone in the reaction equation, while those given per reactive site unit appear multiplied by the number of reactive sites involved.

In this mechanism polymer molecules resulting from termination by combination reactions could contain oxygen atoms in −O−O−, =O or −OH groups that may not react. For that reason, polymer molecules are only identified by their length, regardless of their oxygen content.

It is well known that tertiary atoms are more susceptible to the effects of gamma radiation than secondary ones. The model does not distinguish between the two types of carbon atoms. This is so because the extents of both the scission and crosslinking reactions are several orders of magnitude smaller than the number of tertiary carbon atoms present in the system. Furthermore, those tertiary carbons are distributed randomly among the chains. As a result, our model behaves as if only tertiary carbon atoms could participate in any reaction.

3.2.2. Mass and moment balances

Mass balance equations may be written for all the species involved in the mechanism. They are shown in the Appendix. Since polymers have a length distribution with sizes anywhere between 1 and infinity, there are infinitely many species to be described. Therefore the set of mass balance equations represented by Equations (A.1)–(A.9) is infinitely large. The method of moments is one of the most commonly used techniques to deal with this type of problem. It transforms the original infinitely large problem involving every species in the length distribution into a finite problem involving moments of that distribution. Those moments are enough to calculate average molecular properties. The Appendix shows the corresponding moments for radical and polymer length distributions (Equations (A.10)–(A.13)) as well the resulting transformed balances (Equations (A.1)–(A.4), (A.14)–(A.21)) and details on model implementation.

4. Results

It is well known that polyethylenes, and in particular HPB, are mainly crosslinked by irradiation under vacuum or under inert atmosphere. In air or in the presence of oxygen, scission becomes predominant. The competition between those two reactions determines the evolution of the molecular structure. If scission predominates during the entire process, the molecular weight decreases continuously. If crosslinking predominates molecular weight increases continuously and the system may reach the gel point.

For the experiments performed in this work, the gel point is a function of the initial oxygen concentrations. The evolution of gel fraction with dose is shown in Fig. 1. We may observe that when HPB was irradiated in an oxygen-free atmosphere, the dose of 30 kGy was insufficient to produce a gel, while a significant gel fraction was generated upon irradiating at a level of 56 kGy. As we have no experimental data at intermediate doses, it is difficult to determine accurately the gel point from the available experimental data for pure N_2 atmosphere. However, the dose range where gel appears is in accordance with a critical gel dose of about 50 kGy that can be estimated from previously reported results for HPB having similar chemical composition that were irradiated under vacuum [18]. In order to perform that estimation, we assumed a linear relationship between gel dose and 1/Mw. Beyond the gel point the oxygen-free sample shows the expected behavior of increase of gel fraction with irradiation, reaching 90% gel for an applied dose of 165 kGy.

As the concentration of oxygen in the initial atmosphere increased, the gel point shifted to higher doses. Thus, the critical dose for gelation falls between 80 and 100 kGy for samples irradiated under an atmosphere of 21% initial oxygen, and between 140 and 160 kGy for samples irradiated under atmospheres having 50 and 75% initial oxygen. In the case of the samples irradiated under 100% oxygen, a small amount of gel is first detected at 200 kGy, leading to the conclusion that the gel point is close to this dose.

It is already known that a rather complex oxidation process is initiated when free macroradicals react with oxygen, leading to

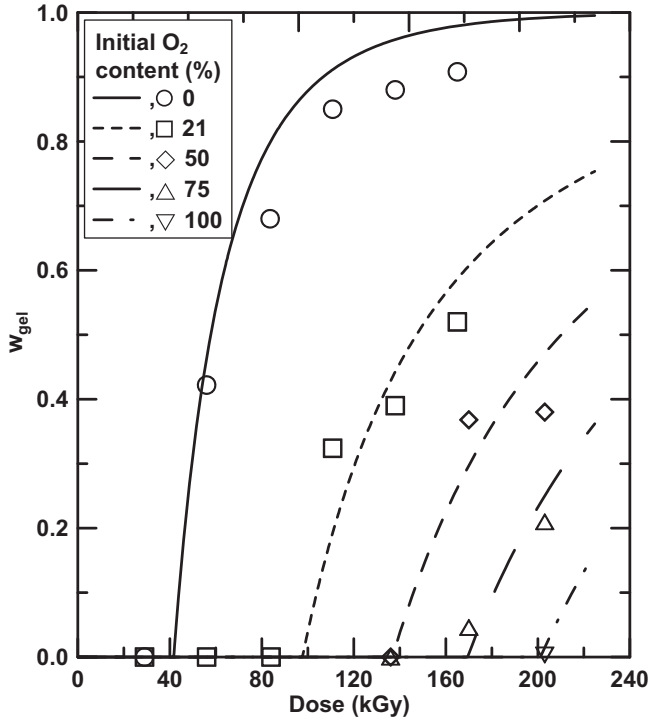

Fig. 1. Evolution of gel fraction with dose. Symbols: experimental measurements; lines: probability model fits.

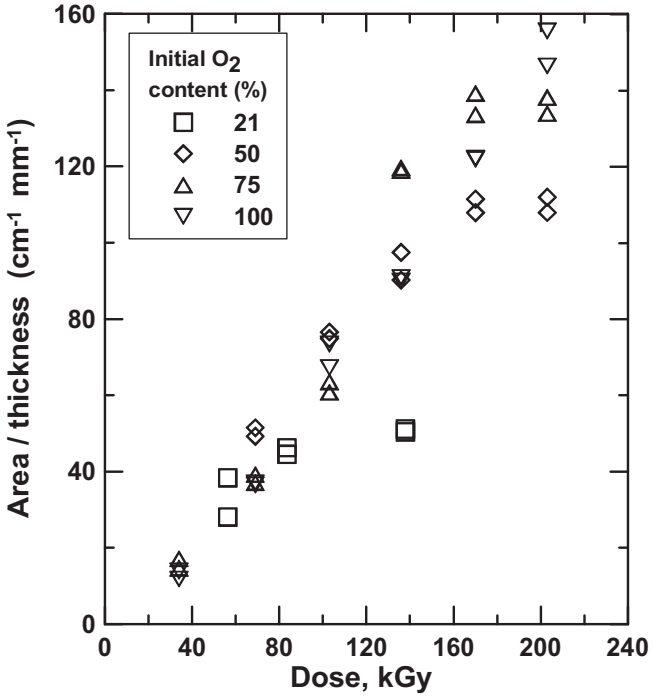

Fig. 2. Area of the absorbance peak center at 1710 cm^{-1} normalized by the film thickness as a function of the dose.

the generation of a great variety of chemical species, such as hydroperoxides, alcohols, acids, and ketones, along with others [8,29,30]. Among the oxidation products, those bearing carbonyl groups can be clearly detected by IR spectroscopy. The IR spectra of the samples irradiated under oxygen atmospheres displayed a set of overlapping absorption bands in the region between 1800 and 1650 cm^{-1} that is ascribed to carbonyl groups [31]. Those bands were absent in the spectra corresponding to the samples irradiated under nitrogen. In order to compare the samples in terms of their oxidation levels, we use a carbonyl index calculated as mentioned in the experimental section. Fig. 2 presents the carbonyl index expressed in absorbance/thickness (cm^{-1} mm^{-1}) units as a function of the applied dose. It can be observed that the index increases with dose. This is in agreement with the results found by other authors [32,33]. As may be observed in Fig. 2, the variation of the carbonyl index with dose is independent of the initial oxygen content up to doses close to the gel point. This is an indication that there is an excess of oxygen in the bulk of material that can react with macroradicals formed in this dose range.

Since the polymer used was practically monodisperse, SEC elution curves were very sensitive to changes in the molecular weight distribution (MWD) induced by the radiation treatment. Figs. 3 and 4 show examples of normalized SEC curves of polymers analyzed after irradiation at various doses under initial atmospheres of either 100% nitrogen or 100% oxygen. The trace of the original narrow distribution HPB polymer is also included as a reference in both figures. In Fig. 3, the only pregel trace corresponds to 29 kGy. The low molecular weight end of this trace shows almost no change. At the high molecular weight end, however, the formation of a population of molecules having molar masses significantly larger than those in the original one may be clearly observed. These new species are a consequence of the termination by combination of macroradicals. On the low molecular end of the traces corresponding to postgel doses (56 and 138 kGy) in Fig. 3, the appearance of a population of molecules shorter than any present in the original distribution may also be seen. These new smaller molecules may only be the result of scission reactions. The high molecular end of each postgel trace still shows a population of molecules larger than those of the virgin polymer. The concentration of those large molecules shows a decrease with irradiation dose. This is so because the postgel traces correspond to the sol fraction only, a fraction of the sample that diminishes with dose as the larger

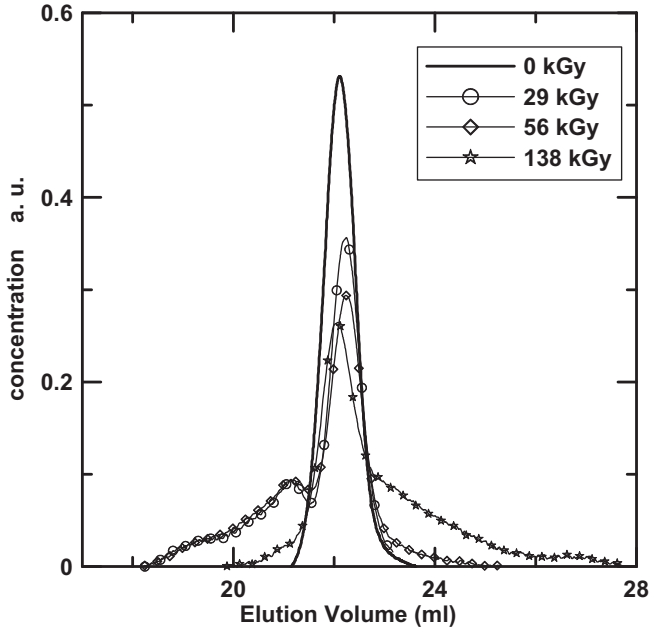

Fig. 3. GPC traces of HPB irradiated under nitrogen atmosphere.

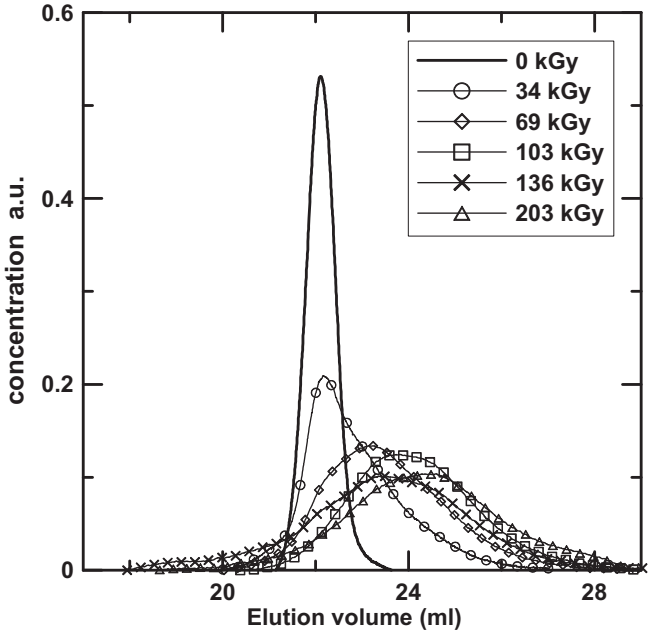

Fig. 4. GPC traces of HPB irradiated under 100% oxygen atmosphere.

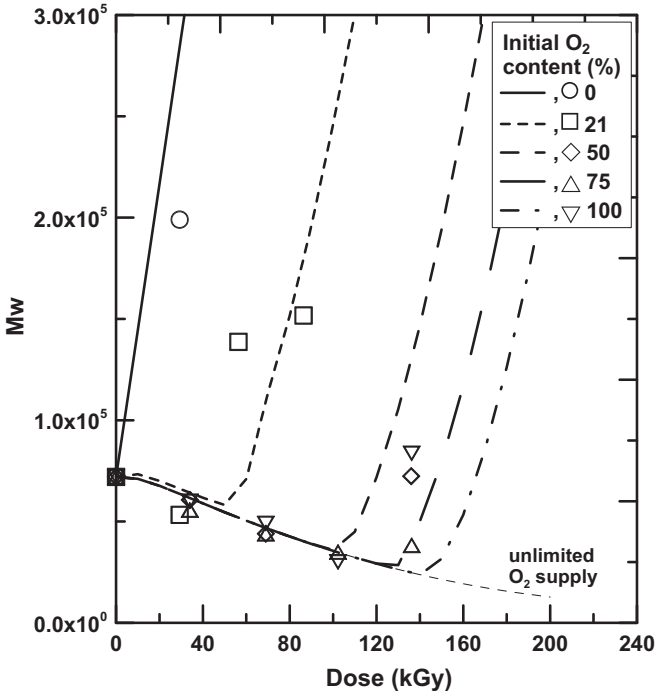

Fig. 5. Weight average molecular weights in the pregel region. Symbols: experimental measurements; lines: kinetic model fits.

molecules become part of the gel. Both pregel and postgel GPC traces clearly confirm that there is a competition between crosslinking and chain scission for this particular system. We have estimated that the mass fraction of scissioned material amounts to about 8% of the modified polymer. We have observed the same qualitative changes in the MWD of HPB irradiated under vacuum [7,18,27]. The traces in Fig. 4 correspond to irradiation under pure oxygen. Only the 203 kGy trace corresponds to a postgel dose. All traces show an increase in the concentration of species shorter than those present in the virgin polymer, a clear indication of scission. There is evidence of a very slight increase of the high molecular weight species, and that only at high doses near the gel point. Comparison between Figs. 3 and 4 leads to the conclusion that scission is much more important under pure oxygen than it is under pure nitrogen, while the opposite is true for crosslinking. Intermediate behaviors are observed in the SEC traces of materials subjected to irradiation at intermediate oxygen contents.

The Mw data corresponding to samples irradiated under oxygen-containing atmospheres show an initial decrease followed by an increase until the gel point, as shown in Figs. 5 and 6. The descending portion of the data appeared to fall on the same curve, regardless of the initial oxygen content in the atmosphere. This indicates that in all cases the amount of oxygen present is enough to inhibit the crosslinking reaction and promote the reactions leading to chain scission. An assumption made in the kinetic model described previously was that the oxygen concentration was similar in all samples. The kinetic rate constants were used as adjustable parameters, the values of which were obtained by fitting the calculated results to the experimental data on Mw. Details on the fitting method may be found in the Appendix. The resulting values are indicated in Table 2. Reported values for the constants are scarce, and at most correspond to particular kinetic steps in the context of different kinetic mechanisms. Any of the reported kinetic mechanisms, including the one in this work, are necessarily simplified versions of a much more complex reality. When fitting the various models to experimental data, any overlooked or lumped steps will affect the values of the kinetic rate constants of every step that was taken into account. For this reason, the kinetic rate constants of like steps found in different kinetic models cannot be compared. The ones obtained in this work only make sense in the context of this particular model.

The resulting fitted molecular weights compare well with the experimental data, as shown in Fig. 5. The largest differences are found close to the gel points, where experimental measurements are prone to higher errors. The curves corresponding to oxygen

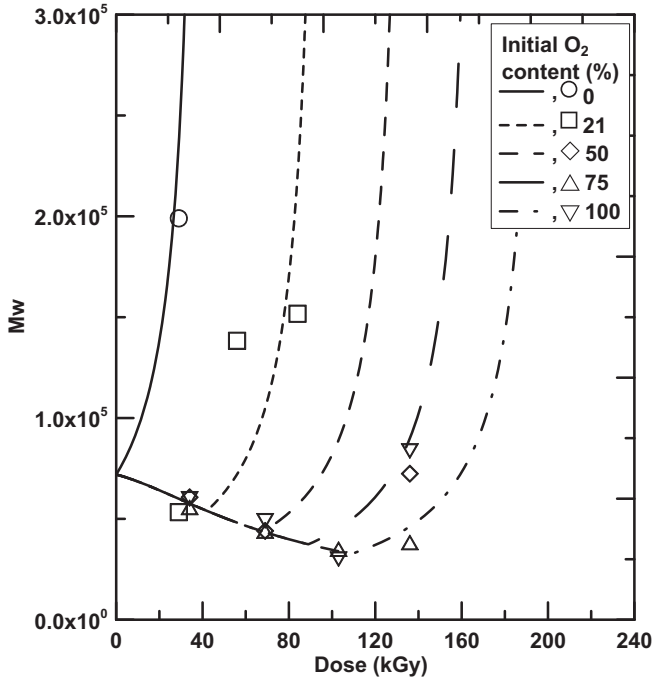

Fig. 6. Weight average molecular weights in the pregel region. Symbols: experimental measurements; lines: probability model predictions.

Table 2
Estimated values of the kinetic rate constants.

Constant	Value (l mol s)
k_v	6.279×10^2
$k_{\gamma a}$	1.101×10^2
k_{or}	7.108×10^3
k_{roo}	3.061×10^0
k_{eo}	3.338×10^{-2}
k_{trr}	7.863×10^0
k_{too}	0.000×10^0
k_{tor}	1.831×10^1
k_{drr}	3.240×10^0
k_{doo}	0.000×10^0
k_{dor}	1.391×10^1
k_{tpr}	2.116×10^2
k_{tpo}	1.356×10^0
k_{tps}	2.170×10^1

containing atmospheres show an initial descent, followed by an increase in the molecular weight. Although the curves do not coincide exactly in the descending portion where scission is predominant, they are very close. Moreover, they practically coincide with the decreasing curve predicted for an atmosphere with an unlimited supply of oxygen, for which the oxygen content in the film would be expected to be constant. The change of regime from mainly scission to mainly crosslinking appears at doses that increase with the initial oxygen content.

Given that the results of the kinetic model indicate that it would be reasonable to assume that Mw curves overlap in the region where oxygen concentration is constant and scission predominates, regardless of initial oxygen content in the gas phase, the nine experimental values of Mw that are smaller than the starting value were used to fit the parameters P_{a1} and P_{b1} in the probability model. The values were found using Marquardt's method for minimizing the objective function.

$$F = \sum_i \left(\mathrm{Mw}_i^{\exp} - \mathrm{Mw}_i^{\mathrm{mod}}\right)^2 \tag{16}$$

where the superscripts 'exp' and 'mod' indicate experimental measurement and model estimation, respectively. The resulting optimal values are $P_{a1} = 6.97068 \times 10^{-6}$, $P_{b1} = 2.5485 \times 10^{-5}$. This indicates that the level of crosslinking, while not zero, is significantly lower than the level of scission. Fig. 6 shows the pregel Mw calculated with these parameters compared to the experimental values. All curves coincide in the descending portion, and show reasonable agreement with the experimental data. The model requires fitting the remaining parameters: P_{a2} and the four $D_{ch,i}$ corresponding to the change of regime of the four oxygen-containing atmospheres used in this work (there is no change of regime for the N_2 atmosphere). In order to do this we used the information on gel fraction, and used Marquardt's method to minimize the objective functions

$$F_i = \sum_j \left(w_{sol,i}^{\exp} - w_{sol,i}^{\mathrm{mod}}\right)_j^2 \quad i = 1\ldots4; j = 1\ldots6 \tag{17}$$

where the subscript i identifies each of the four oxygen-containing atmospheres, and the subscript j identifies the irradiation doses used. The resulting parameters are $P_{a2} = 9.33 \times 10^{-6}$, and the $D_{ch,i}$ indicated in Table 3.

The resulting gel fraction fits are shown in Fig. 1, where a good agreement with the experimental data is obtained. The dose at which the regime changes from mainly scission to mainly crosslinking is predicted to increase with the initial O_2 content, in agreement with the findings from the kinetic model. The relationship is linear in the oxygen-containing atmospheres. This suggests that the change of regime is related to the depletion of O_2 in the system.

Table 3
Estimated values of the change of regime dose for different starting atmospheres.

O_2 content (%)	$D_{ch,i}$ (kGy)
0	0
21	42
50	68
75	88
100	109

5. Conclusions

We have used a γ source to irradiate practically monodisperse HPB in sealed glass ampoules containing different concentrations of O_2, in several doses up to 200 kGy. We found that in the oxygen-free atmosphere the molecular weight increases up to the gel point, while in every oxygen-containing atmosphere the treatment results in an initial decrease of molecular weight, followed by an increase up to the gel point. This suggests that the limited amount of oxygen present in the ampoules is consumed in the process.

We also present two complementary mathematical models to treat the data and try to gain insight in the process. The models agree well with the experimental data, suggesting that their underlying assumptions are reasonable: the concentration of O_2 is constant in the solid HPB as long as the gas phase acts as a reservoir, and then diminishes to extinction.

Acknowledgments

The authors wish to thank the support of CONICET, ANPCyT (gs2) and Universidad Nacional del Sur (gs3).

Appendix A

A.1. Mass balance equations

Oxygen in the gas phase

$$V^g \frac{d\left[O_2^g\right]}{dt} = V^f r_o^f \quad V^g O_2^g \geq V^f O_2^f \tag{A.1}$$

$$V^g \frac{d\left[O_2^g\right]}{dt} = -k_v\left(\left[O_2^g\right] - \left[O_2^f\right]\right) \quad V^g O_2^g < V^f O_2^f \tag{A.2}$$

Oxygen in the film phase

$$V^f \frac{d\left[O_2^f\right]}{dt} = 0 \quad V^g O_2^g \geq V^f O_2^f \tag{A.3}$$

$$V^f \frac{d\left[O_2^f\right]}{dt} = k_v\left(\left[O_2^g\right] - \left[O_2^f\right]\right) + r_o^f V^f \quad V^g O_2^g < V^f O_2^f \tag{A.4}$$

$$r_o^f = -k_{or}\left[O_2^f\right]\left(\sum_{n=1}^{\infty}[R_n]\right) + (k_{too} + k_{doo} + k_{roo})\left(\sum_{n=1}^{\infty}[R_n]\right)^2 \tag{A.5}$$

Polymer with n monomer units ($n = 1\ldots\infty$)

$$\begin{aligned}\frac{d[P_n]}{dt} = &-k_{\gamma a} n[P_n] + k_{so}\sum_{m=n+1}^{\infty}[R_mO] \\ &+\frac{1}{2}k_{trr}\sum_{m=1}^{n-1}[R_{n-m}][R_m](1-\delta_{n,1}) \\ &+k_{tor}\sum_{m=1}^{n-1}[R_{n-m}][R_mO_2](1-\delta_{n,1}) \\ &+\frac{1}{2}k_{too}\sum_{m=1}^{n-1}[R_{n-m}O_2][R_mO_2](1-\delta_{n,1}) + k_{drr}[R_n]\sum_{m=1}^{\infty}[R_m] \\ &+k_{dor}\left([R_n]\sum_{m=1}^{\infty}[R_mO_2] + [R_nO_2]\sum_{m=1}^{\infty}[R_m]\right) \\ &+k_{doo}[R_nO_2]\sum_{m=1}^{\infty}[R_mO_2] + k_{tpr}\left(\sum_{m=1}^{\infty}m[P_m]\right)[R_n] \\ &-k_{tpr}n[P_n]\left(\sum_{m=1}^{\infty}[R_m]\right) + k_{tpo2}\left(\sum_{m=1}^{\infty}m[P_m]\right)[R_nO_2] \\ &-k_{tpo2}n[P_n]\left(\sum_{m=1}^{\infty}[R_mO_2]\right) + k_{tpo}\left(\sum_{m=1}^{\infty}m[P_m]\right)[R_nO] \\ &-k_{tpo}n[P_n]\left(\sum_{m=1}^{\infty}[R_mO]\right)\end{aligned} \tag{A.6}$$

Backbone radical with n monomer units ($n = 1\ldots\infty$)

$$\begin{aligned}\frac{d[R_n]}{dt} = &\,k_{\gamma a} n[P_n] - k_{or}\left[O_2^f\right][R_n] + k_{eo}\sum_{m=n+1}^{\infty}[R_mO] + k_{tpr}n[P_n] \\ &\times\left(\sum_{m=1}^{\infty}[R_m]\right) - k_{tpr}\left(\sum_{m=1}^{\infty}m[P_m]\right)[R_n] + k_{tpo2}n[P_n] \\ &\times\left(\sum_{m=1}^{\infty}[R_mO_2]\right) + k_{tpo}n[P_n]\left(\sum_{m=1}^{\infty}[R_mO]\right) \\ &-(k_{trr}+k_{drr})[R_n]\sum_{m=1}^{\infty}[R_m] \\ &-(k_{tor}+k_{dor})[R_n]\sum_{m=1}^{\infty}[R_mO_2]\end{aligned} \tag{A.7}$$

Peroxy-radical with n monomer units ($n = 1\ldots\infty$)

$$\begin{aligned}\frac{d[R_nO_2]}{dt} = &\,k_{or}\left[O_2^f\right][R_n] - k_{tpo2}\left(\sum_{m=1}^{\infty}m[P_m]\right)[R_nO_2] \\ &-(k_{tor}+k_{dor})[R_nO_2]\sum_{m=1}^{\infty}[R_m] - (k_{too}+k_{doo} \\ &+k_{roo})\left[R_nO_2\right]\sum_{m=1}^{\infty}[R_mO_2]\end{aligned} \tag{A.8}$$

Oxy-radical molecules with n monomer units ($n = 1\ldots\infty$)

$$\begin{aligned}\frac{d[R_nO]}{dt} = &\,k_{roo}[R_nO_2]\left(\sum_{m=1}^{\infty}[R_mO_2]\right) - k_{tpo}\left(\sum_{m=1}^{\infty}m[P_m]\right)[R_nO] \\ &-k_{so}[R_nO]\end{aligned} \tag{A.9}$$

A.2. Moment definitions

ath order moment for polymer

$$M_a = \sum_{n=1}^{\infty} n^a[P_n] \quad a = 0,1,2\ldots; \tag{A.10}$$

ath order moment for backbone radicals

$$Y_a = \sum_{n=1}^{\infty} n^a[R_n] \quad a = 0,1,2\ldots \tag{A.11}$$

ath, order moment for peroxy-radicals

$$Z_a = \sum_{n=1}^{\infty} n^a[R_nO_2] \quad a = 0,1,2\ldots \tag{A.12}$$

ath, order moment for oxy-radicals

$$S_a = \sum_{n=1}^{\infty} n^a[R_nO] \quad a = 0,1,2\ldots \tag{A.13}$$

Moment balance equations are obtained by transforming mass balances as follows. Equations (A.6)–(A.9) must be multiplied by n^a, and then added up for all possible lengths, measured as monomeric units in the species. Equation (A.5) is also rearranged as a function of those moments, since their expressions appear directly in this balance. After the transformation stage, the resulting oxygen reaction term and the moment balances are those shown in Equations (A.14)–(A.18).

$$r_o^f = -k_{or}\left[O_2^f\right]Y_0 + (k_{too}+k_{doo}+k_{roo})Z_0^2 \tag{A.14}$$

ath moment for polymer ($a = 0,1,2$)

$$\begin{aligned}\frac{dM_a}{dt} = &-k_{\gamma a}M_{a+1} + k_{eo}W_a + \frac{1}{2}k_{trr}Q_{rr,a} + k_{tor}Q_{or,a} + \frac{1}{2}k_{too}Q_{oo,a} \\ &+k_{drr}Y_aY_0 + k_{dor}(Y_aZ_0 + Z_aY_0) + k_{doo}Z_aZ_0 + k_{tpr}M_1Y_a \\ &-k_{tpr}M_{a+1}Y_0 + k_{tpo2}M_1Z_a - k_{tpo2}M_{a+1}Z_0 + k_{tpo}M_1S_a \\ &-k_{tpo}M_{a+1}S_0\end{aligned} \tag{A.15}$$

ath moment for backbone macroradical ($a = 0,1,2$)

$$\begin{aligned}\frac{dY_a}{dt} = &\,k_{\gamma a}M_{a+1} - k_{or}\left[O_2^f\right]Y_a + k_{eo}W_a + k_{tpr}M_{a+1}Y_0 - k_{tpr}M_1Y_a \\ &+k_{tpo2}M_{a+1}Z_0 + k_{tpo}M_{a+1}S_0 - (k_{trr}+k_{drr})Y_aY_0 \\ &-(k_{tor}+k_{dor})Y_aZ_0\end{aligned} \tag{A.16}$$

ath moment for peroxy-macroradical

$$\begin{aligned}\frac{dZ_a}{dt} = &\,k_{or}O_2^fY_a - k_{tpo2}M_1Z_a - (k_{tor}+k_{dor})Z_aY_0 - (k_{too}+k_{doo} \\ &+k_{roo})Z_aZ_0\end{aligned} \tag{A.17}$$

ath moment for oxy-macroradical

$$\frac{dS_a}{dt} = k_{roo}Z_aZ_0 - k_{tpo}M_1S_0 - k_{so}S_a \tag{A.18}$$

where:

$$W_a = \sum_{n=1}^{\infty}n^a\sum_{t=n+1}^{\infty}[R_tO] = \sum_{t=2}^{\infty}\left(\sum_{n=1}^{t-1}n^a\right)[R_tO]$$

$$W_0 = \sum_{t=2}^{\infty}(t-1)[P_t] = M_1 - M_0;\; W_1 = \sum_{t=2}^{\infty}(t^2-t)\left[P_t\right] = \frac{M_2-M_1}{2}$$

$$W_2 = \sum_{t=2}^{\infty}\left(\frac{1}{3}t^3 - \frac{1}{2}t^2 + \frac{1}{6}t\right)\left[P_t\right] = \frac{1}{3}M_3 - \frac{1}{2}M_2 + \frac{1}{6}M_1$$

$$\begin{aligned}Q_{rr,a} &= \sum_{n=1}^{\infty}n^a\sum_{m=1}^{n-1}[R_{n-m}][R_m](1-\delta_{n,1}) \\ &= \sum_{n=2}^{\infty}n^a\sum_{m=1}^{n-1}[R_{n-m}][R_m] = \sum_{m=1}^{\infty}\sum_{n=m+1}^{\infty}n^a[R_{n-m}][R_m] \\ &= \sum_{m=1}^{\infty}\sum_{u=1}^{\infty}(u+m)^a[R_u][R_m];\; Q_{rr,a} = \sum_{m=1}^{\infty}\sum_{k=0}^{a}\binom{a}{k}Y_kY_{a-k}\end{aligned}$$

Similarly, $Q_{oo,a} = \sum_{m=1}^{\infty} \sum_{k=0}^{a} \binom{a}{k} Z_k Z_{a-k}$ and $Q_{or,a} = \sum_{m=1}^{\infty} \sum_{k=0}^{a} \binom{a}{k} Z_k Y_{a-k}$

Since the resulting expressions depend on moments of orders that are higher than those included in the balances, a closure technique [34] must be used. We employ the log-normal distribution assumption for the length of the molecule. Its selection was based on the inspection of the shape of experimental MWDs of the modified resins. Moreover, we and other authors successfully employed this assumption to describe polymerization a modification process where PE is involved [28,35]. The expression used in the estimation of the third moment in length is shown in Equation (A.19).

$$M_3 = \frac{M_2}{M_1} M_0 \tag{A.19}$$

Once the various moments are calculated, the following measurable quantities may be calculated.

Number-average molecular weight

$$\mathrm{Mn} = 28 \frac{M_1 + Y_1 + Z_1 + S_1}{M_0 + Y_0 + Z_0 + S_0} \tag{A.20}$$

Weight-average molecular weight

$$\mathrm{Mw} = 28 \frac{M_2 + Y_2 + Z_2 + S_2}{M_1 + Y_1 + Z_1 + S_1} \tag{A.21}$$

Equations (A.1)–(A.4), (A.14)–(A.21) constitute a stiff algebraic-differential system which is solved numerically in the gPROMS environment (Process System Enterprise, Inc.).

The model needs the following input data: mass of unmodified polymer, the molecular weight of the repeat unit in the polymer chain, the virgin resin average molecular weights (M_n and M_w), the mass fraction of oxygen in the gas phase, the operating temperature and the residence time. The model also requires the values of the kinetic parameters. They were estimated by fitting the model to experimental information as described in the next section.

A.3. Kinetic parameter estimation.

The kinetic constants were estimated using the tools of the gPROMS program, imposing as a condition that the predictions of the model should fit the measured average molecular weights of the irradiated samples in the pregel region (see Table 1).

The gPROMS parameter estimator uses the following objective function:

$$F = K + \frac{1}{2} \min_{S} \sum_{i=1}^{N_{tot}} \ln\left(\sigma_i^2\right) + \frac{\left(y_i^{meas} - y_i^{calc}\right)^2}{\sigma_i^2} \tag{A.22}$$

where K is a constant calculated as a function of the total number of measurements (N_{tot}) involved in the estimation, S is the set of model parameters to be estimated, σ_i^2 is the variance of the ith measurement, y_i^{meas} is the ith measured value and y_i^{calc} is the ith calculated value. The variances are calculated as $\sigma_i^2 = \omega^2 (y_i^{meas} + \varepsilon)^{\gamma}$, where ω and γ are adjustable parameters, and ε is a very small number related to machine accuracy.

References

[1] Matsuo H, Dole M. Irradiation of polyethylene. IV. Oxidation effects. J Phys Chem 1959;63:837–43.

[2] Giberson RC. Oxygen diffusion and reaction during γ-irradiation of polyethylene. J Phys Chem 1962;66:463–8.

[3] Seguchi T, Arakawa K, Hayakawa N, Watanabe Y, Kuriyama I. Radiation induced oxidative degradation of polymers-II. Effects of radiation on swelling and gel fraction of polymers. Radiat Phys Chem 1982;19:321–7.

[4] Arakawa K, Seguchi T, Watanabe Y, Hayakawa N. Radiation-Induced oxidation of polyethylene, ethylene-butene copolymer, and ethylene-propylene copolymer. J Polym Sci A-Polym Chem 1982;20:2681–92.

[5] Tidjani A, Arnaud R. Gamma-oxidation of linear low density polyethylenes: ethylene–butene and ethylene–hexene copolymers. J Polym Sci Part A: Polym Chem 1993;31:603–9.

[6] Kang HY, Saito O, Dole M. The radiation chemistry of polyethylene. IX. Temperature coefficient of cross-linking and other effects. J Am Chem Soc 1967;89:1980–6.

[7] Andreucetti NA, Curzio OA, Vallés EM, Carella JM. Structural changes induced by γ-rays on model linear ethylene-butene copolymers. Int J Radiat Appl Intrum C Radiat Phys Chem 1988;31:663–70.

[8] Decker C, Mayo FR, Richardson H. Aging and degradation of polyolefins - 3. Polyethylene and ethylene-propylene copolymers. J Polym Sci A-Polym Chem 1973;11:2879–98.

[9] Khelidj N, Colin X, Audouin L, Verdu J, Monchy-Leroy C, Prunier V. Oxidation of polyethylene under irradiation at low temperature and low dose rate. Part I. the case of "pure" radiochemical initiation. Polym Degrad Stabil 2006;91:1593–7.

[10] Buttafava A, Tavares A, Arimondi M, Zaopo A, Nesti S, Dondi D, et al. Dose rate effects on the radiation induced oxidation of polyethylene. Nucl Instrum Meth Phys Res B 2007;265:221–6.

[11] Kitamaru R, Mandelkern L. Irradiation cross linking of polyethylene. The temperature dependence of cross linking in the crystalline and amorphous states. J Am Chem Soc 1964;86:3529–34.

[12] Dalinkevich AA, Piskarev IM, Shlyapnikov YA. On the mechanism of initiation in the radiation-induced oxidation of polyethylene. Polym Degrad Stabil 1993;40:117–9.

[13] Failla MD, Vallés EM, Lyons BJ. Effect of initial crystallinity on the response of high-density polyethylene to high-Energy radiation. J Appl Polym Sci 1999;71:1375–84.

[14] Arakawa K, Seguchi T, Hayakawa N, Machi S. Radiation-Induced oxidation of polymers. Effect of antioxidant and antirad agent on oxygen consumption and gas evolution. J Polym Sci A-Polym Chem 1983;21:1173–81.

[15] Arakawa K, Seguchi T, Watanabe Y, Hayakawa N, Kuriyama I, Machi S. Dose rate effect on radiation-induced oxidation of polyethylene and ethylene-propylene copolymer. J Polym Sci A-Polym Chem 1981;19:2123–5.

[16] Babić D. The influence of oxygen on radiation crosslinking and degradation of polymers at low irradiation doses. Makromol Chem Macromol Symp 1989;28:231–47.

[17] Babić D. Crosslinking and scission of polyethylene at low irradiation doses. Int J Radiat Appl Intrum C Radiat Phys Chem 1990;35:158–62.

[18] Andreucetti N, Fernández Lagos L, Curzio O, Sarmoria C, Vallés E. Model linear ethylene-butene copolymers irradiated with γ-rays. Polymer 1999;40:3443–50.

[19] Tripodi S, Carella JM, Curzio OA, Valles EM. Molecular weight and antioxidant effects on the structure of irradiated linear low density polyethylene. Radiat Phys Chem 1991;38:89–94.

[20] Morton M, Fetters LJ. Anionic polymerization of vinyl monomers. Rubber Chem Technol 1975;48:359–409.

[21] Rachapudy H, Smith GG, Raju VR, Graessley WW. Properties of amorphous and crystallization hydrocarbon polymers - 3. Studies of the hydrogenation of polybutadiene. J Polym Sci B-Polym Phys 1979;17:1211–22.

[22] Carella JM, Graessley WW, Fetters LJ. Effects of chain microstructure on the viscoelastic properties of linear polymer melts: polybutadienes and hydrogenated polybutadienes. Macromolecules 1984;17:2775–86.

[23] Silverstein RM, Morrill TC, Bassler C. Spectrometric identification of organic compounds. New York: John Wiley & Sons; 1963.

[24] Dintcheva NT, Al-Malaika S, La Mantia FP. Effect of extrusion and photo-oxidation on polyethylene/clay nanocomposites. Polym Degrad Stabil 2009;94:1571–88.

[25] Kurtz SM, Muratoglu OK, Buchanan FJ, Currier B, Gsell R, Shen FW, et al. Interlaboratory studies to determine optimal analytical methods for measuring the oxidation index of UHMWPE. Biomaterials 2001;22:2875–81.

[26] Vallés E, Sarmoria C, Villar M, Lazzari M, Chiantore O. Model polydimethylsiloxanes subjected to thermal weathering: effect on molecular weight distributions. Polym Degrad Stabil 2000;69:67–71.

[27] Andreucetti NA, Sarmoria C, Curzio OA, Vallés EM. Effect of the phenolic antioxidants on the structure of gamma- irradiated model polyethylene. Radiat Phys Chem 1998;52:177–82.

[28] Pedernera MN, Sarmoria C, Vallés EM, Brandolin A. Improved kinetic model for the peroxide initiated modification of polyethylene. Polym Eng Sci 1999;39:2085–95.

[29] Dole M. The radiation chemistry of macromolecules. New York: Academic Press; 1972.

[30] Zenkiewicz M, Rauchfleisz M, Czuprynska J. Comparison of some oxidation effects in polyethylene film irradiated with electron beam or gamma rays. Radiat Phys Chem 2003;68:799–809.

[31] Silverstein RM, Morrill TC, Bassler C. Spectrometric identification of organic compounds. 5th ed. New York: John Wiley & Sons, Inc; 1991.

[32] Lacoste J, Carlsson DJ. Gamma-, photo-, and thermally-initiated oxidation of linear low density polyethylene: a quantitative comparison of oxidation products. J Polym Sci A-Polym Chem 1992;30:493–500.
[33] Audouin-Jirackova L, Papet G, Verdu J. Effect of radiochemical ageing on the tensile properties of high density polyethylene. Eur Polym J 1989;25:181–6.
[34] Hulburt HM, Katz S. Some problems in particle technology. A statistical mechanical formulation. Chem Eng Sci 1964;19:555–74.
[35] Zabisky RCM, Chan WM, Gloor PE, Hamielec AE. A kinetic model for olefin polymerization in high-pressure tubular reactors: a review and update. Polymer 1992;33:2243–62.